Myeloid-derived MIF drives RIPK1-mediated cerebromicrovascular endothelial cell death to exacerbate ischemic brain injury

Yan Li[a,1], Chengyu Zou[b,c,1], Chen Chen[a], Sixuan Li[b], Ziyu Zhu[a], Qiuyue Fan[a], Rui Pang[a], Fengshi Li[d], Zengai Chen[e], Zhenghong Wang[a], Weifeng Yu[a], Junying Yuan[b,c,2] (ORCID), and Peiying Li[a,2]

Macrophage migration inhibitory factor (MIF) is a multifaced protein that plays important roles in multiple inflammatory conditions. However, the role of MIF in endothelial cell (EC) death under inflammatory condition remains largely unknown. Here we show that MIF actively promotes receptor-interacting protein kinase 1 (RIPK1)-mediated cell death under oxygen-glucose deprivation condition. MIF expression is induced by surgical trauma in peripheral myeloid cells both in perioperative humans and mice. We demonstrate that MIF-loaded myeloid cells induced by peripheral surgery adhere to the brain ECs after distal middle cerebral artery occlusion (dMCAO) and exacerbate the blood–brain barrier (BBB) disruption. Genetic depletion of myeloid-derived MIF in perioperative ischemic stroke (PIS) mice with MCAO following a surgical insult leads to significant reduction in ECs apoptosis and necroptosis and the associated BBB disruption. The adoptive transfer of peripheral blood mononuclear cells (PBMC) from surgical MIF$^{\Delta Lyz2}$ mice to wild-type (WT) MCAO mice also shows reduced ECs apoptosis and necroptosis compared to the transfer of PBMC from surgical MIF$^{fl/fl}$ mice to MCAO recipients. The genetic inhibition of RIPK1 also attenuates BBB disruption and ECs death compared to that of WT mice in PIS. The administration of MIF inhibitor (ISO-1) and RIPK1 inhibitor (Nec-1s) can both reduce the brain EC death and neurological deficits following PIS. We conclude that myeloid-derived MIF promotes ECs apoptosis and necroptosis through RIPK1 kinase-dependent pathway. The above findings may provide insights into the mechanism as how peripheral inflammation promotes the pathology in central nervous system.

MIF | inflammation | RIPK1 | stroke | cell death

The blood–brain barrier (BBB) is a unique microvasculature system that functions as a critical brain–blood interface that protects the integrity and homeostasis of central nervous system (CNS). Investigating the mechanism that maintains the integrity of BBB is crucial for us to understand the regulation of the exchange between CNS and periphery in health and disease. In particular, peripheral inflammation, such as the activation of the innate or adaptive immune system and release of proinflammatory cytokines, can perturb the function of CNS and promote pathology. Understanding the mechanism by which peripheral inflammation promotes CNS pathology is relevant to a multitude of human diseases, particularly neurodegenerative diseases. Perioperative ischemic stroke (PIS), defined as any stroke that occurs within 30 d of the initial surgical procedure, involves the interaction of peripheral inflammation induced by a sterile surgical procedure with the CNS (1–3). The incidence of PIS can be as high as 1.9 to 9.7% after major peripheral vascular and cardiac surgeries (4, 5) and 0.1 to 1.9% among non-cardiac, non-neurological surgical patients (4). The mortality of PIS can be as high as 60% (4). Importantly, PIS may provide a good model for us to understand the mechanism by which peripheral inflammation promotes CNS pathology. Investigating the mechanism of PIS may not only help to improve postoperative management but also provide valuable insights into the mechanism by which the peripheral inflammation promotes the CNS pathology.

The endothelial cells (ECs) that line the walls of cerebromicrovasculature form the key part of the BBB (6, 7). Damage to cerebromicrovascular ECs by ischemic brain injury can promote neural dysfunction and cognitive impairment (8–10). The cellular homeostasis and survival of cerebromicrovascular ECs can be impaired by various pathological conditions, including oxidative stress, inflammation, and trauma (11) and consequently, leading to EC death (12, 13). Surgical trauma has recently been highlighted as an important inducer of sterile inflammation by promoting the release of pro-inflammatory cytokines, such as interleukin-1β (IL-1β), tumor necrosis factor (TNF-α), interleukin-6 (IL-6), interleukin-8 (IL-8), and interferon-γ (14). However, it is unclear how surgically induced inflammation in the peripheral tissues may promote the damage to cerebrovascular ECs and induce pathology in the CNS.

Significance

The role of peripheral inflammation in promoting CNS pathology is relevant to a wide range of human neurological conditions. Our study implicates the role of peripheral myeloid-derived MIF in driving the pathological progression of perioperative stroke (PIS), defined as any stroke that occurs within 30 d of a peripheral surgical procedure, a condition affecting 0.1 to 1.9% non-cardiac, non-neurologic, non-major surgical patients and up to 10% high-risk cardiac or brain surgical patients worldwide. We show activation of RIPK1 by myeloid-derived MIF in promoting cerebromicrovascular EC apoptosis and necroptosis. Our results suggest that MIF and RIPK1 can serve as promising therapeutic targets for preserving cerebromicrovascular EC survival and BBB integrity in CNS pathologies promoted by peripheral inflammation.

[1]Y.L. and C.Z. contributed equally to this work.

[2]To whom correspondence may be addressed. Email: junying_yuan@sioc.ac.cn or peiyingli.md@gmail.com.

Macrophage migration inhibitory factor (MIF) is a multifunctional cytokine that has been suggested to play important roles in cardiovascular diseases, autoimmune diseases, sepsis, pneumonia, diabetes, and neurodegenerative diseases such as Parkinson's disease (15–18). Classically known as a centrally important driver of local and systemic inflammation, MIF acts as an inflammatory and stress-regulating cytokine with chemokine-like functions and is rapidly released in response to various stimuli including surgery (19) to directly or indirectly promote the production or expression of a large panel of pro-inflammatory molecules, such as TNF-α, IL-1, IL-6, IL-8 (20, 21). Macrophages are an abundant and important source of MIF (22). In response to various activating ligands, such as damage-associated molecular patterns, pathogen-associated molecular patterns, and environmental metabolic changes, MIF could also be upregulated in myeloid and lymphocyte lineage cell types to mediate cell death under different conditions (23–27). However, the role of MIF in EC death remains largely unknown.

Receptor-interacting protein kinase 1 (RIPK1) has been established as a key mediator of TNFR1 signaling (28). Classically, stimulation of TNFR1 by its cognate ligand TNF leads to the recruitment and activation of RIPK1 which in turn mediates multiple deleterious responses, including inflammation and cell death (28, 29). The activation of RIPK1 downstream of TNFR1 may mediate RIPK1-dependent apoptosis (RDA) in apoptotic competent cells, or necroptosis under apoptosis-deficient conditions (29). RIPK1 can be activated in cerebrovascular ECs by cerebral ischemic brain insult to mediate cell death (30). Inhibition of RIPK1 reduces brain pathology after ischemic insult (31). However, the pathway that leads to the activation of RIPK1 after cerebral ischemic brain insult remains unclear. Importantly, interaction of MIF with RIPK1 has not been investigated.

We find that MIF can promote the activation of RIPK1 in oxygen–glucose deprivation condition in cultured cells. We further investigate the functions of MIF and RIPK1 in vivo using conditional knockout MIF$^{\Delta Lyz2}$ mice and RIPK1 kinase-dead knockin RIPK1$^{D138N/D138N}$ mice. We find that macrophage-derived MIF can induce RIPK1-dependent EC necroptosis and apoptosis in PIS model. Genetic deletion or pharmacological blockage of MIF and RIPK1 kinase activity reduces cell death of cerebral ECs and the associated BBB disruption and neurological deficits after PIS. Our study elucidates a previously unrecognized mechanism of MIF-induced ECs necroptosis and apoptosis under surgical trauma-induced sterile inflammation. Our findings suggest that MIF and RIPK1 may serve as novel therapeutic targets to reduce BBB disruption and neurological dysfunction after PIS or other CNS pathology induced by peripheral inflammation.

Results

MIF Promotes RIPK1 Activation and EC Cell Death under Oxygen and Glucose Deprivation (OGD).

To understand the function of MIF on EC cell death following ischemic injury, we determined the death of bEnd3 cells treated with OGD for 6 h followed by reoxygenation for 24 h. We found that increased numbers of TUNEL$^+$ CD31$^+$ cells after rMIF treatment upon OGD and the TUNEL$^+$ CD31$^+$ cells could be antagonized by administrating with MIF inhibitor (S,R)3-(4-hydroxyphenyl)-4,5-dihydro-5-isoxazole acetic acid methyl ester(ISO-1) (Fig. 1A). However, no TUNEL$^+$ CD31$^+$ cells were found under non-OGD condition with rMIF or ISO-1 treatment (Fig. 1A). This data suggests that MIF may play an important role in cell death under OGD condition.

Since cerebral ischemic insult can lead to reduction in the levels of TAK1 to sensitize RIPK1-mediated cell death (30), we next investigated the impact of OGD on TAK1 levels in bEnd3 cells. We found that the TAK1 expression was significantly reduced in bEnd3 cells following OGD (Fig. 1B). Furthermore, treatment with MIF induced the death of bEnd3 cells under OGD condition during re-oxygenation phase in a time-dependent manner, which was inhibited by RIPK1 inhibitor R-7-Cl O-necrostatin-1 (Nec-1s). The activation of RIPK1 kinase activity and the apoptosis biomarker cleaved-caspase-3 (CC3) in bEnd3 cells under OGD condition during re-oxygenation phase was rescued by Nec-1s (Fig. 1 C–E). The sensitization of RIPK1 and CC3 activation by MIF under OGD condition could be blocked by the MIF inhibitor ISO-1 (Fig. 1E).

Collectively, the above data suggest that MIF can induce EC cell death under OGD condition by promoting RIPK1 activation.

Increased Peripheral Myeloid-MIF Expression after Surgical Trauma in Human and Mice.

Sterile inflammation after surgical procedures elicits not only peripheral immune responses, but can also induce remarkable neuroinflammation in CNS (32). To examine the change of MIF levels in response to the surgical stimuli, we prospectively recruited surgical patients (*SI Appendix*, Table S1) and collected peripheral blood samples before surgery and 24 h after surgery. The absolute numbers and the percentages of both MIF$^+$ classical macrophages (MIF$^+$CD16$^-$) and non-classical macrophages (MIF$^+$CD16$^+$) in peripheral blood were significantly increased after surgery compared to that of the pre-surgical levels (Fig. 2 A–C). The plasma levels of MIF measured by enzyme-linked immunosorbent assay (ELISA) were also significantly increased after surgery (Fig. 2D).

We next investigated the role of MIF in PIS using mouse as a model. Mice were either subjected to surgery alone (4 d before sample collection) or PIS in which mice were subjected to surgery 1 d prior to distal middle cerebral artery occlusion (dMCAO) followed by sample collection 3 d after dMCAO (Fig. 2E). We found that both the absolute number and the percentage of MIF$^+$F4/80$^+$ macrophages in blood were significantly increased in the surgery-alone group compared to that of control group (Fig. 2 F and G). The above changes were also found in PIS mice compared to that of IS alone alone group 3 d after dMCAO (Fig. 2 F and G), but not in the blood collected at 1 d after dMCAO from PIS mice (*SI Appendix*, Fig. S1A). The increases in the numbers of MIF$^+$F4/80$^+$ macrophages were accompanied by the increase of F4/80$^+$CD11b$^+$ macrophages in the surgery alone and PIS mice (Fig. 2H and *SI Appendix*, Fig. S1B). Thus, the peripheral surgery alone could induce the increases of MIF$^+$F4/80$^+$ macrophages in the peripheral blood. The plasma levels of MIF were also increased in PIS mice compared to the IS mice 3 d after dMCAO (Fig. 2I), but not 1 or 7 d after dMCAO (*SI Appendix*, Fig. S1C). In contrast, the expression levels of MIF in macrophage in spleen (*SI Appendix*, Fig. S1 D and E) and other immune cells in peripheral, such as Ly6G$^+$ neutrophils remained unchanged between IS and PIS groups (*SI Appendix*, Fig. S1 F and G), suggesting MIF induction in peripheral myeloid cells (mainly macrophages) in response to surgery. We further compared the impact of different perioperative factors that could affect patient outcome on the expression of MIF expression using different paradigms and found mice in the surgery and trauma group, but not the pain or stress groups exhibited significantly increased MIF expression in peripheral macrophages compared to the control mice (Fig. 2J). Thus, surgical trauma is a potent inducer of MIF expression in peripheral myeloid cells.
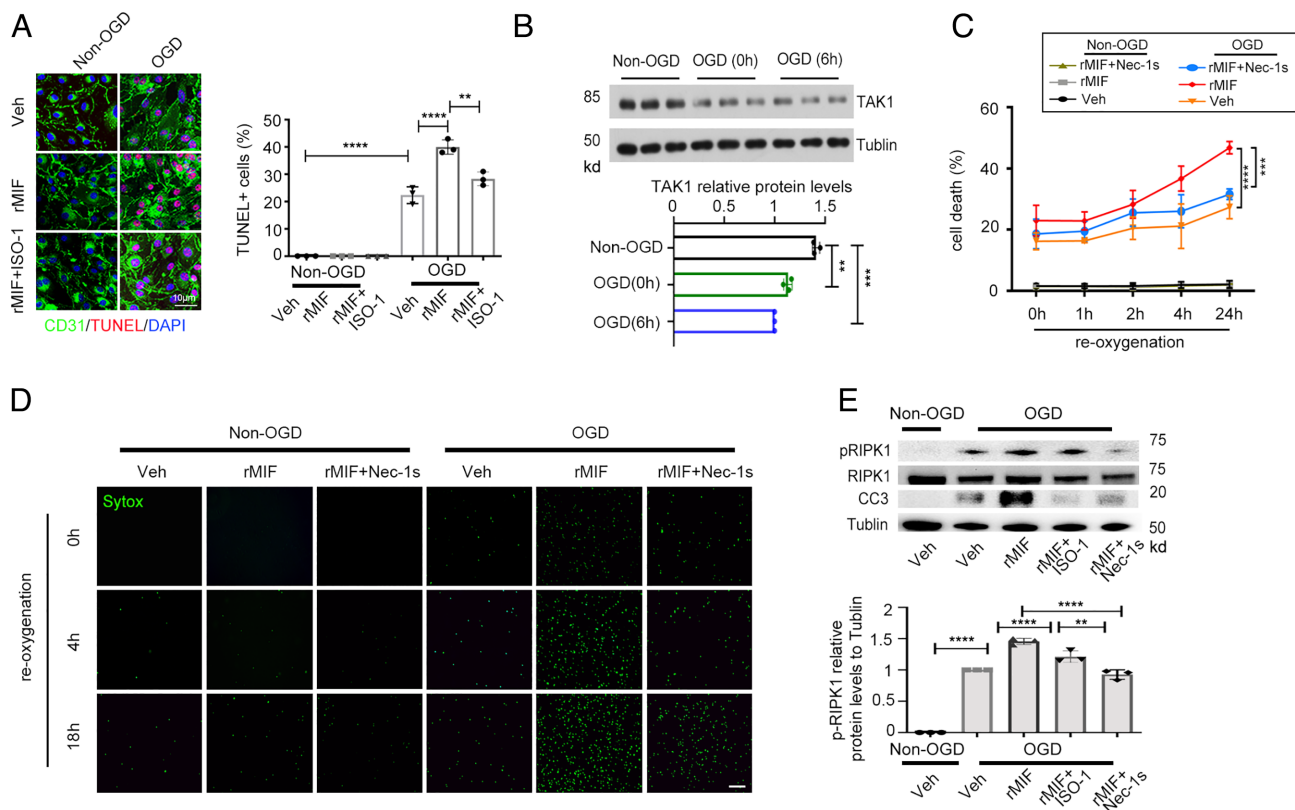
Fig. 1. MIF promotes RIPK1 activation and EC cell death under OGD. (*A*) bEnd3 cells were treated with Vehicle (Veh), 100 ng/mL rMIF or 30 μg/mL (S,R)3-(4-hydroxyphenyl)-4,5-dihydro-5-isoxazole acetic acid methyl ester(ISO-1) under Non-OGD or at onset of OGD (6 h) and the cells were analyzed after reoxygenation phase (24 h). Representative confocal images of TUNEL⁺CD31⁺ bEnd3 cells after treatment with Veh, rMIF or ISO-1 as indicated group. (Scale bar, 10 μm.) Quantification of the percentage of TUNEL⁺bEnd3 cells in each group (n = 3 per group, one-way ANOVA with Bonferroni multiple comparisons test). (*B*) bEnd3 cells subjected to Non-OGD or OGD (0 h, 6 h) were analyzed by immunoblotting for TAK1. Tubulin was used as a loading control. The quantification of western immunoblotting for TAK1 in each group (n = 3 per group, one-way ANOVA with Bonferroni multiple comparisons test). Data are normalized to OGD. (*C*) bEnd3 cells were treated with Veh, 100 ng/mL rMIF or 20 mM Nec-1s at onset of OGD (6 h) and the cells were analyzed during reoxygenation phase (0, 1, 2, 4, and 24 h). bEnd3 cells were treated with Veh, 100 ng/mL rMIF or 20 mM Nec-1s under Non-OGD for the same period of time. Cell death was measured by SytoxGreen positivity assay. (n = 3 per group, two-way ANOVA with Bonferroni multiple comparisons test). (*D*) Representative staining images of SytoxGreen positive of bEnd3 cells during reoxygenation phase (0, 4, and 18 h) as indicated groups. (Scale bar, 40 μm.) (*E*) Representative western blot images of pRIPK1(pS166), RIPK1, Cleaved-caspase3 (CC3) in the bEnd3 cells treated with Non-OGD+Veh, OGD+Veh, OGD+rMIF, OGD+rMIF+ISO-1, and OGD+rMIF+Nec-1s. Quantification of western immunoblotting for pRIPK1(pS166) in each group (n = 3 per group, one-way ANOVA with Bonferroni multiple comparisons test). All data are expressed as mean ± SD. **$P \leq 0.01$, ***$P \leq 0.001$, ****$P \leq 0.0001$.

PIS Promotes Adhesion of Myeloid Cells to the Cerebromicrovascular ECs. Adhesion of peripheral immune cells to the cerebromicrovascular ECs following brain injuries profoundly contributes to the BBB disruption (33). Using two-photon in vivo imaging, we found that PIS mice had significantly increased adhesion of Rhodamine 6G-stained cells (mainly neutrophils and macrophages), indicating the increased presence of peripheral myeloid cells (34, 35) on the ischemic cerebromicrovascular ECs compared to that of IS mice (Fig. 3*A*) (Movies S1–S3). The adhesion of Rhodamine 6G-stained cells on brain ECs peaked at 3 d following dMCAO in PIS mice, which was consistent with the MIF expression in peripheral myeloid cells following PIS as measured by flow cytometry (Fig. 3*B*) and immunofluorescent staining (Fig. 3*C* and *SI Appendix,* Fig. S2A). RNA scope analysis revealed that the levels of MIF messenger RNA (mRNA) were significantly increased in Iba1⁺ cells around ECs in the brains of PIS mice compared to that in the IS or sham mouse brains (Fig. 3*D*). These data suggest that circulating myeloid cells could be the major source of the elevated MIF levels detected around the cerebromicrovascular ECs.

We next evaluated the impact of peripheral surgery on stroke in the CNS using T2-weighted imaging, dynamic contrast-enhanced-MRI analysis. We found that PIS mice developed larger infarct volumes (Fig. 3*E*) as well as higher volume transfer constants (K^trans), extravascular space volume ratio (RVE), and plasma

volume ratio values (RVP) as compared to that of IS mice (Fig. 3*E*), suggesting exacerbated BBB disruption in PIS mice. We also found a significant increase of IgG extravasation in PIS mice 3 and 7 d but not 1 d after dMCAO (*SI Appendix,* Fig. S3 *A and B*). Moreover, IgG immunofluorescent staining did not reveal significant differences in the extent of BBB destruction between 14 and 28 d after dMCAO (*SI Appendix,* Fig. S3B). Supporting PIS-mediated damage to ECs, the levels of tight junction protein zonula occludens-1 (ZO-1) were significantly reduced in PIS mice 3 d after dMCAO compared with IS mice (Fig. 3*F*). Taken together, these multiple independent lines of evidence suggest that PIS promotes the adhesion of myeloid cells to ECs in ischemic brains and exacerbates BBB disruption.

Myeloid-Derived MIF Mediates Apoptosis and Necroptosis of ECs in PIS. To examine the contribution of surgically induced MIF in peripheral myeloid cells to cerebromicrovascular EC death, we generated MIF^fl/fl mice using CRISPR-Cas9 (*SI Appendix,* Fig. S4 *A–C*) and crossed with Lyz-cre mice to generate the myeloid-specific deletion of MIF in MIF^ΔLyz2 (MIF^fl/fl; Lyz2^cre) mice (Fig. 4*A* and *SI Appendix,* Fig. S4 *D and E*). The increases in CC3⁺ and TUNEL⁺ brain ECs following PIS were significantly reduced in MIF^ΔLyz2 mice as compared to that of MIF^fl/fl mice (Fig. 4*B* and *SI Appendix,* Fig. S5 *A–C*). Since MIF induced RIPK1 activation
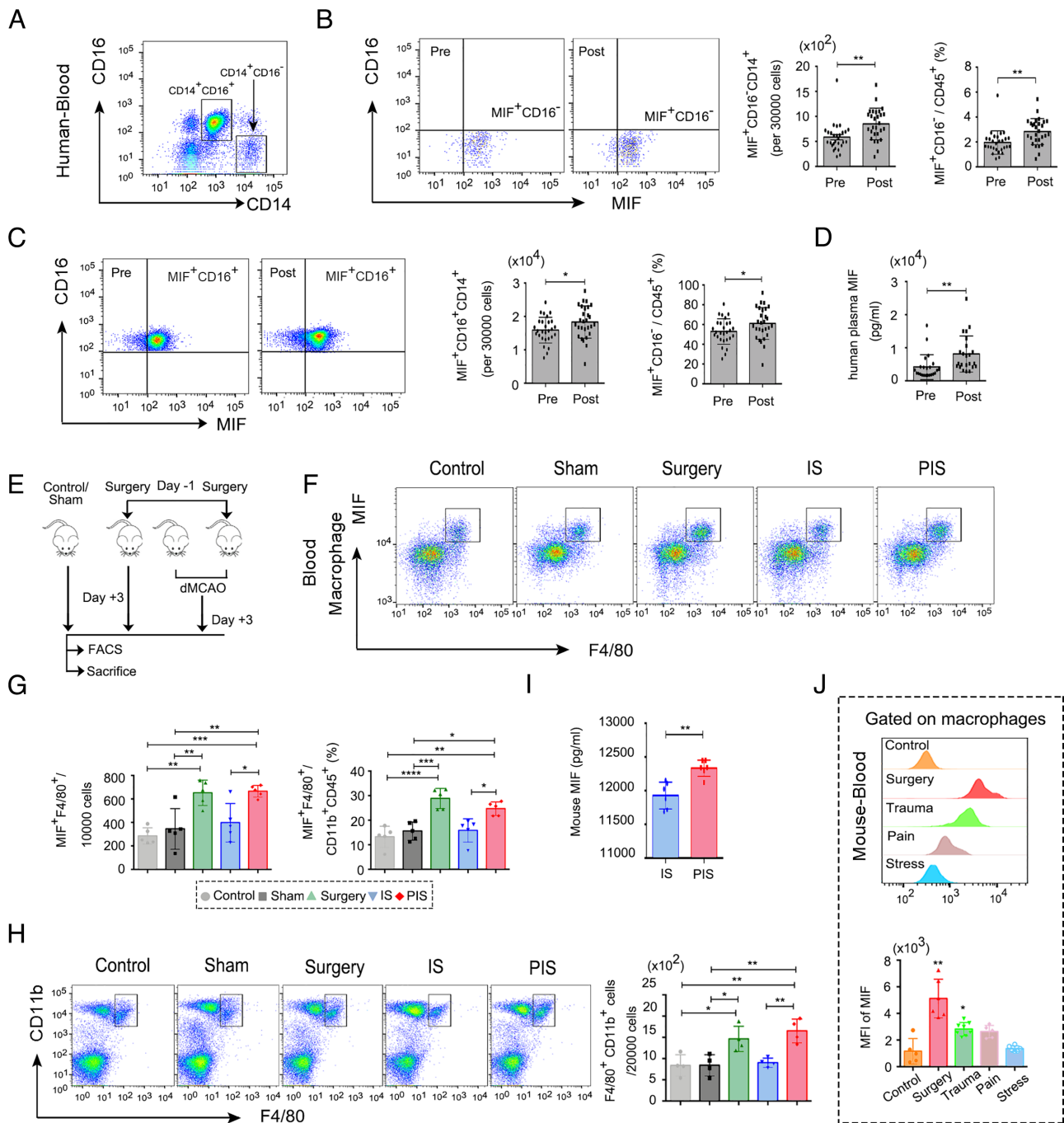
Fig. 2. Increased MIF expression in peripheral myeloid cells after surgical trauma both in human and mice. (*A*) Gating of classical or non-classical monocytes from human peripheral white blood cells. (*B*) Representative images (*Left*) and quantification (*Right*) of MIF expression in classical monocytes in the blood of patients before and 1 d after surgery (n = 23 for surgery patients, unpaired Student's *t* test). (*C*) Representative images (*Left*) and quantification (*Right*) of MIF expression in non-classical monocytes in the blood of patients before and 1 d after surgery (n = 23 for surgery patients, unpaired Student's *t* test). (*D*) Peripheral levels of MIF were quantified by ELISA in the plasma of patients before and 1 d after surgery (n = 23 for surgery patients, unpaired Student's *t* test). (*E*) Experimental design for PIS in WT mice. (*F*) Flow cytometry analysis of MIF⁺ F4/80⁺CD11b⁺CD45⁺ cells in the peripheral blood of control, sham, surgery, IS and PIS mice 3 d after dMCAO. (*G*) Quantification of MIF⁺F4/80⁺ cells among CD11b⁺CD45⁺ cells in F (n = 5 per group, one-way ANOVA with Bonferroni multiple comparisons test). (*H*) Flow cytometry analysis (*Left*) and quantification (*Right*) of F4/80⁺CD11b⁺CD45⁺ cells in the peripheral blood of control, sham, surgery, IS and PIS mice 3 d after dMCAO (n = 4 per group, one-way ANOVA with Bonferroni multiple comparisons test). (*I*) Peripheral levels of MIF were quantified by ELISA in the plasma 3 d after dMCAO (n = 6 per group, unpaired Student's *t* test). (*J*) Representative histogram (*Up*) and quantification (*Down*) of MIF expression in macrophages in the blood of mice from control, surgery, trauma, pain, and stress groups 3 d after surgery (n = 5 to 8 per group, one-way ANOVA with Bonferroni multiple comparisons test). All data are expressed as mean ± SD. *$P \leq 0.05$, **$P \leq 0.01$, ***$P \leq 0.001$, ****$P \leq 0.0001$.

and promoted RIPK1-dependent cell death in OGD (Fig. 1), we further examined the levels of pRIPK1, pRIPK3, and pMLKL, biomarkers for necroptosis, in cerebromicrovascular ECs after PIS. The levels of pRIPK1, pRIPK3, and pMLKL were increased in the ECs after PIS compared to those in IS mice (*SI Appendix*, Fig. S5 *D* and *E*), but significantly reduced in the ECs of MIF$^{\Delta Lyz2}$ mice

compared with that of MIF$^{fl/fl}$ mice (Fig. 4 *C–E*). Thus, MIF derived from myeloid cells is important in inducing the activation of RIPK1 and cell death including both apoptosis and necroptosis.

To further address whether surgery-induced myeloid-derived MIF mediated the cell death of cerebromicrovascular ECs after stroke, we performed surgery on donor mice (MIF$^{\Delta Lyz2}$ mice or
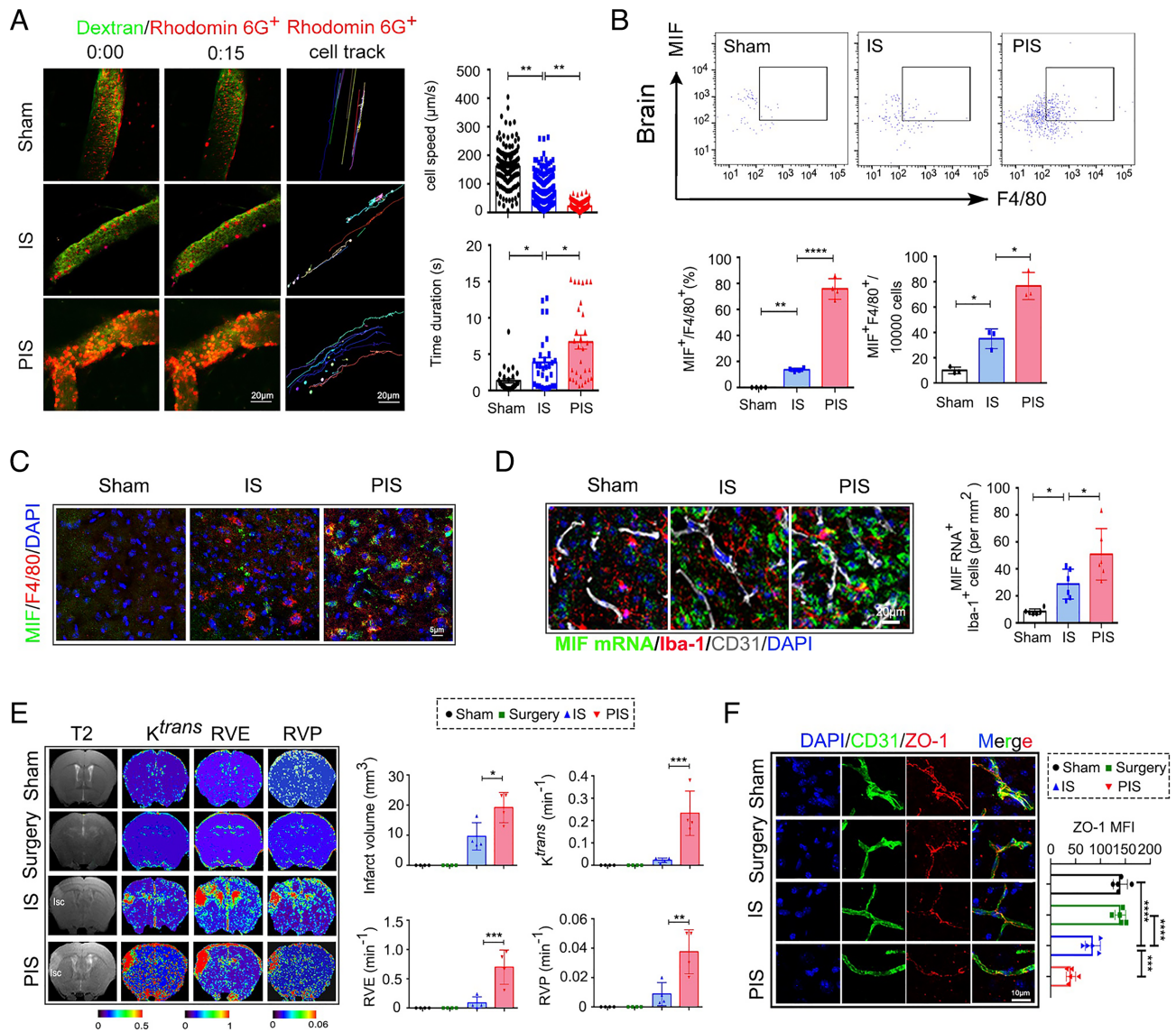
Fig. 3. PIS promotes adhesion of myeloid cells to the cerebromicrovascular ECs. (*A*) Representative two-photon time lapse in vivo images (*Left*) of Rhodamine 6G-stained cells recruitment in the brain of sham and IS, PIS mice 3 d after dMCAO. Images are representative of 2 animals/group. (Scale bar, 20 μm.) (*Right*) Quantification of the moving speed of Rhodamine 6G stained cells in the ischemic brain region (200 cells per group in two mice, one-way ANOVA with Bonferroni multiple comparisons test). (*Right*) Quantification of the interaction between Rhodamine 6G-stained cells and the vasculature during a 15 s interval (30 cells per group in two mice, one-way ANOVA with Bonferroni multiple comparisons test). (*B*) Flow cytometry analysis (*Up*) of MIF$^+$ F4/80$^+$CD11b$^+$CD45$^+$ cells in brain of sham, IS and PIS mice 3 d after dMCAO. (*Down*) The percentage and absolute numbers of MIF$^+$ F4/80$^+$CD11b$^+$CD45$^+$ cells in brain as indicated groups (n = 3 to 4 per group, one-way ANOVA with Bonferroni multiple comparisons test). (*C*) Representative confocal images of MIF and F4/80 double immunostaining of indicated group. (Scale bar, 5 μm.) (*D*) Representative images of RNA scope (*Up*) show the expression of MIF mRNA in brain ECs and Iba-1$^+$ cells from sham, IS and PIS mice. (Scale bar, 20 μm.) (*Down*) Quantification of MIF$^+$ mRNA Iba-1$^+$ cells in the brain sections from sham, IS and PIS mice. (n = 6 per group, one-way ANOVA with Bonferroni multiple comparisons test). (*E*) Typical evolution pattern of T2-weighted imaging, volume transfer constants (K^{trans}), extravascular space volume ratio (RVE), plasma volume ratio values (RVP) in 7 T MRI, indicating infarct volume and BBB disruption at 3 d after dMCAO in sham, IS, and PIS mice. Blue color represents low permeability and red represents higher permeability. The quantification of infarct volume, volume transfer constants (K^{trans}), extravascular space volume ratio (RVE), and plasma volume ratio values (RVP) values in the cortex of sham, IS mice and PIS mice (n = 4 per group, one-way ANOVA with Bonferroni multiple comparisons test). (*F*) Representative Z-stack confocal images of the tight junction protein ZO-1 and ECs marker CD31 in brain sections obtained from sham, surgery, IS and PIS mice 3 d after dMCAO. (Scale bar, 10 μm.) Quantification of ZO-1 MFI of indicated groups (n = 5 per group, one-way ANOVA with Bonferroni multiple comparisons test). All data are expressed as mean ± SD. *$P \leq 0.05$, **$P \leq 0.01$, ***$P \leq 0.001$,****$P \leq 0.0001$.

MIF$^{fl/fl}$ mice). The peripheral blood mononuclear cells (PBMC), collected and purified 1 d after surgery, were transferred into wild-type (WT) recipient mice 2 h before conducting dMCAO (Fig. 4*F*). The levels of CC3$^+$ ECs, pRIPK1$^+$ ECs, and pRIPK3$^+$ ECs in ischemic brain 3 d after dMCAO were significantly lower in mice receiving PBMCs from MIF$^{\Delta Lyz2}$ mice, compared with that of mice receiving PBMCs from MIF$^{fl/fl}$ mice (Fig. 4*G*). Thus, surgery-induced myeloid-MIF can promote cerebromicrovascular ECs after IS.

To further examine the role of RIPK1 in cerebromicrovascular EC death, we subjected RIPK1$^{D138N/D138N}$ mice to PIS (Fig. 4*H*). While the inhibition of RIPK1 did not affect the levels of MIF, the levels of necroptosis markers, pRIPK1, pRIPK3, and pMLKL were significantly decreased in the cerebromicrovascular ECs of RIPK1$^{D138N/D138N}$ mice (Fig. 4 *I* and *J*). These data suggest that peripheral myeloid-derived MIF is an upstream regulator of RIPK1 in cerebromicrovascular ECs and promotes RIPK1-depedent apoptosis and necroptosis after PIS.
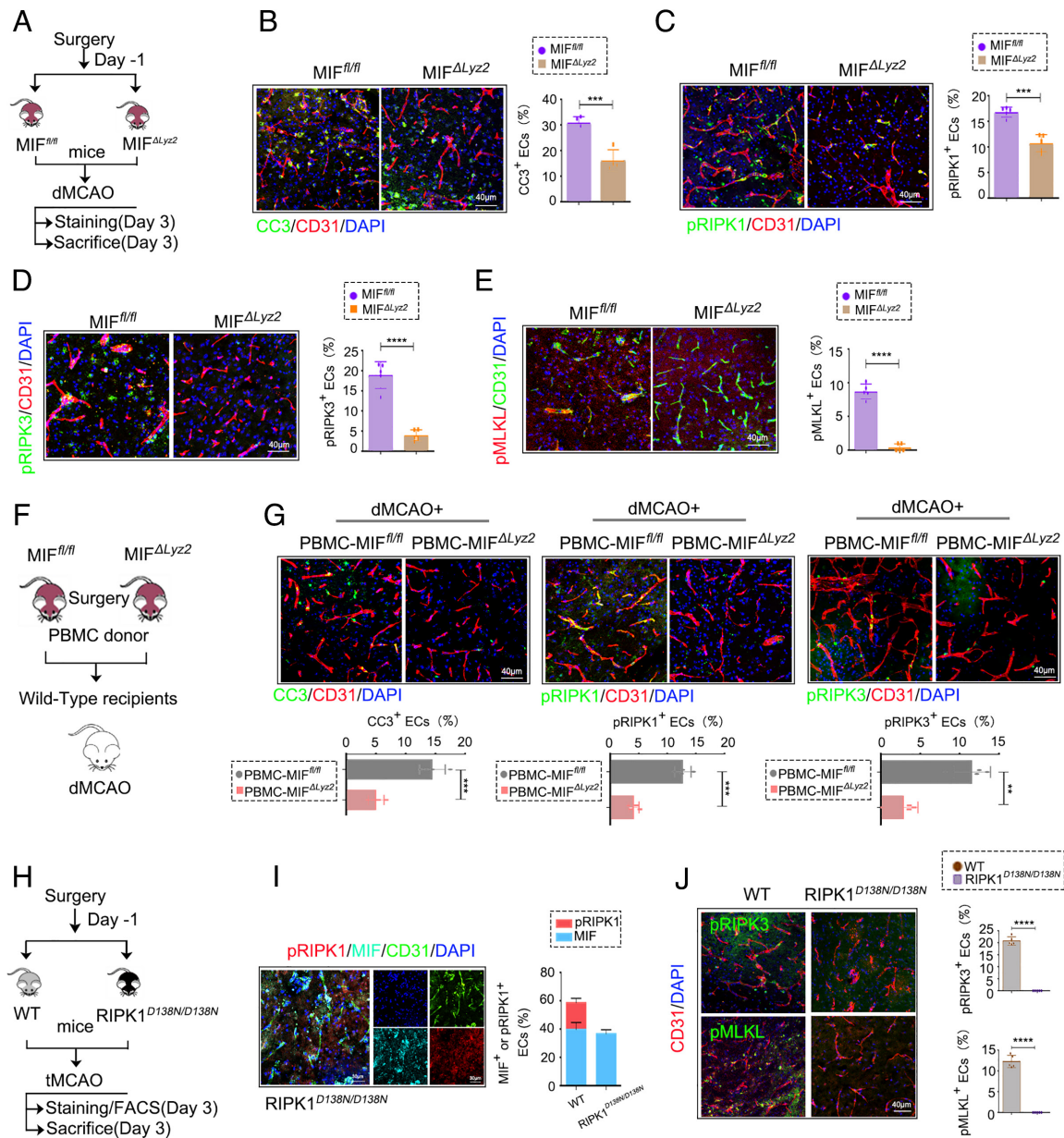
Fig. 4. Myeloid-derived MIF mediates ECs apoptosis and necroptosis in PIS. (*A*) Experimental design for PIS in MIF*fl/fl* and Lyz2*cre*MIF*fl/fl* (MIF*ΔLyz2*) mice. (*B*) Representative confocal images (*Left*) and quantification (*Right*) of CC3+CD31+ ECs of MIF*fl/fl* and MIF*ΔLyz2* PIS mice 3 d after dMCAO. (Scale bar, 40 μm.) CC3+ ECs were quantified (n = 4 per group, unpaired Student's *t* test). (*C*) Representative confocal images (*Left*) and quantification (*Right*) of pRIPK1(pS166)+CD31+ ECs of MIF*fl/fl* and MIF*ΔLyz2* PIS mice 3 d after dMCAO. (Scale bar, 40 μm.) pRIPK1(pS166)+ ECs were quantified. (n = 5 per group, unpaired Student's *t* test). (*D*) Representative confocal images (*Left*) and quantification (*Right*) of pRIPK3(pT231/S232)+CD31+ ECs of MIF*fl/fl* and MIF*ΔLyz2*PIS mice 3 d after dMCAO. (Scale bar, 40 μm.) pRIPK3(pT231/S232)+ ECs were quantified. (n = 5 per group, unpaired Student's *t* test). (*E*) Representative confocal images (*Left*) and quantification (*Right*) of pMLKL(pSer345)+CD31+ ECs of MIF*fl/fl* and MIF*ΔLyz2* PIS mice 3 d after dMCAO. (Scale bar, 40 μm.) pMLKL(pSer345)+ ECs were quantified. (n = 5 per group, unpaired Student's *t* test). (*F*) As indicated in the experimental scheme. donor mice (MIF*ΔLyz2* mice and MIF*fl/fl* mice) were subjected to BF, and 1 d later their PBMC were transplanted to WT dMCAO mice. (*G*) Representative confocal images of CC3+CD31+ECs, pRIPK1(pS166)+CD31+ECs, pRIPK3(pT231/S232)+CD31+ ECs in brain sections obtained from dMCAO+PBMC- MIF*fl/fl* and dMCAO+PBMC-MIF*ΔLyz2*recipient mice. (Scale bar, 40 μm.) CC3+ ECs, pRIPK1(pS166)+ ECs, pRIPK3(pT231/S232)+ ECs were quantified. (n = 4 per group, unpaired Student's *t* test). (*H*) Experimental design for PIS in WT and RIPK1*D138N/D138N* mice. (*I*) Representative confocal images of pRIPK1(pS166), MIF and CD31 in brain sections obtained from RIPK1*D138N/D138N* PIS mice 3 d after tMCAO. (Scale bar, 30 μm.) (n = 5 per group, unpaired Student's *t* test). (*J*) Representative confocal images (*Left*) and quantification (*Right*) of pRIPK3(pT231/S232)+CD31+ ECs and pMLKL(pSer345)+CD31+ ECs in brain sections obtained from WT and RIPK1*D138N/D138N* PIS mice 3 d after tMCAO. (Scale bar, 40 μm.) pRIPK3(pT231/S232)+ ECs and pMLKL(pSer345)+ ECs were quantified. (n = 5 per group, unpaired Student's *t* test). Data are represented as mean ± SD. **$P \leq 0.01$, ***$P \leq 0.001$, ****$P \leq 0.0001$.

Myeloid MIF Deficiency and RIPK1 Kinase Inhibition Reduce BBB Disruption after PIS. Given the important role of ECs on the maintenance of BBB integrity, we compared the response of MIF*fl/fl* mice and MIF*ΔLyz2* mice to PIS. Compared to that of MIF*fl/fl* mice, MIF*ΔLyz2* mice developed smaller infarct volume and reduced the extravasation of IgG after PIS (Fig. 5*A*). The loss of ZO-1 and sensorimotor deficits measured by adhesive removal test were reduced in MIF*ΔLyz2* mice as compared to those in MIF*fl/fl*

mice following PIS (Fig. 5 *B* and *C*). IS (dMCAO) mice receiving PBMCs from MIF*ΔLyz2* mice before the procedure exhibited smaller infarct volume, less extravasation of IgG (Fig. 5*D*), and loss of ZO-1 (Fig. 5*E*) as compared to that of dMCAO mice receiving PBMCs from MIF*fl/fl* mice. Thus, myeloid-derived MIF alone may be able to induce damage in cerebromicrovascular ECs in stroke.

We next examined the role of MIF on cultured EC line bEnd3 cells. When PBMCs isolated from the mice after surgery were
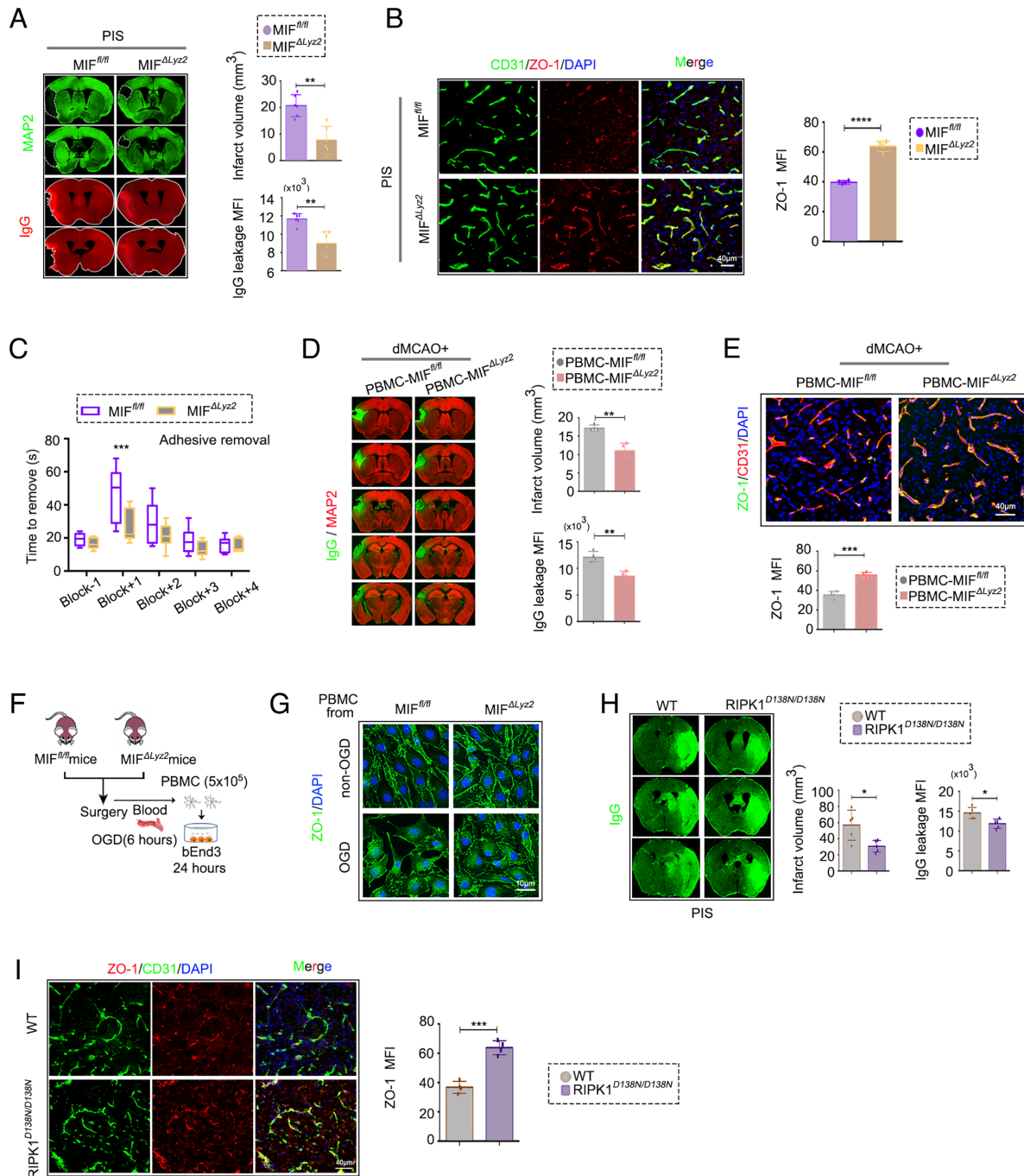
Fig. 5. Myeloid MIF deficiency and RIPK1 kinase inhibition reduces BBB disruption after PIS. (*A*) Representative MAP2 images of the lesion (*Up*) and endogenous IgG extravasation staining (*Down*) in MIF$^{fl/fl}$ and MIF$^{\Delta Lyz2}$ PIS mice 3 d after dMCAO. Quantification of infarct volume and IgG leakage MFI of indicated groups. (n = 6 per group, unpaired Student's *t* test). (*B*) Representative confocal images of the tight junction protein ZO-1 and CD31 in brain sections obtained from MIF$^{fl/fl}$ and MIF$^{\Delta Lyz2}$ PIS mice 3 d after dMCAO. (Scale bar, 40 μm.) Quantification of ZO-1 MFI of indicated groups. (n = 4 per group, unpaired Student's *t* test). (*C*) Sensorimotor functions were assessed using the adhesive removal test in MIF$^{fl/fl}$ and MIF$^{\Delta Lyz2}$ PIS mice. (n = 8 per group, two-way ANOVA with Bonferroni multiple comparisons test). (*D*) Representative MAP2(red)/IgG(green) images (*Left*) of the lesion in dMCAO+PBMC-MIF$^{fl/fl}$ and dMCAO+PBMC-MIF$^{\Delta Lyz2}$ recipient mice. (*Right*) Quantification of infarct volume and IgG leakage MFI of indicated groups. (n = 4 per group, unpaired Student's *t* test). (*E*) Representative confocal images of the tight junction protein ZO-1 and CD31 in brain sections obtained from dMCAO+PBMC-MIF$^{fl/fl}$ and dMCAO+PBMC-MIF$^{\Delta Lyz2}$ recipient mice. (Scale bar, 40 μm.) Quantification of ZO-1 MFI of indicated groups. (n = 4 per group, unpaired Student's *t* test). (*F*) bEnd3 cells were subject to Non-OGD or OGD (6 h). PBMC obtained from MIF$^{fl/fl}$ and MIF$^{\Delta Lyz2}$ surgery mice and co-cultured with bEnd3 cells during reoxygenation phase (24 h). (*G*) Representative images of ZO-1 immunostaining in the bEnd3 cells after cocultured with PBMC of the indicated groups. (Scale bar, 10 μm.) (*H*) Representative endogenous IgG extravasation (*Left*), infarct volume (*Middle*) and quantification of IgG leakage (*Right*) in WT and RIPK1$^{D138N/D138N}$ mice PIS mice 3 d after tMCAO. (n = 5 per group, unpaired Student's *t* test). (*I*) Representative confocal images of the tight junction protein ZO-1 and CD31 in brain sections obtained from WT and RIPK1$^{D138N/D138N}$ PIS mice 3 d after tMCAO. (Scale bar, 40 μm.) Quantification of ZO-1 MFI of indicated groups. (n = 4 per group, unpaired Student's *t* test). Data are represented as mean ± SD. *$P \leq 0.05$, **$P \leq 0.01$, ***$P \leq 0.001$, ****$P \leq 0.0001$.

co-cultured with bEnd3 cells challenged with OGD (Fig. 5*F*), we found the ZO-1 in bEnd3 cells co-cultured with PBMCs from MIF$^{\Delta Lyz2}$ mice after surgery was significantly preserved compared to those co-cultured with PBMCs from MIF$^{fl/fl}$ mice (Fig. 5*G* and *SI Appendix,* Fig. S6*A*). The addition of rMIF to the bEnd3 cells under OGD condition significantly accelerated the loss of ZO-1

compared to that of OGD insult alone, while the loss of ZO-1 was reduced by adding the MIF inhibitor ISO-1 (*SI Appendix*, Fig. S6 *B* and *C*).

To further examine the role of RIPK1 in the exacerbated BBB disruption following PIS, we subjected RIPK1$^{D138N/D138N}$ mice to PIS and found RIPK1$^{D138N/D138N}$ mice also developed significantly smaller infarct volumes and attenuated BBB damage as detected by endogenous IgG extravasation (Fig. 5*H*) and ZO-1 loss (Fig. 5*I*) compared to that of WT mice. Collectively, our data suggest that myeloid-specific MIF deficiency and inhibition of RIPK1 kinase can both reduce BBB disruption after PIS.

Inhibition of MIF or RIPK1 Reduces PIS-Induced BBB Damage and Neurological Deficit. To examine the effect of pharmacological inhibition of MIF or RIPK1 on BBB disruption after PIS, we administered MIF inhibitor ISO-1 (3 mg/kg) or Nec-1s (10 mg/kg) 2 h before dMCAO in IS or PIS mice (Fig. 6*A*). We found that both the infarct volume (Fig. 6*B*) and the leakage of IgG were reduced after treatment with ISO-1 or Nec-1s in PIS mice as compared to

the treatment of Veh (Fig. 6*C*) and the disruption of tight junction protein ZO-1 was restored with the treatment of ISO-1 or Nec-1s in PIS mice (Fig. 6*D*), while the IS mice administered with rMIF (60 μg/kg) exhibited similar extent of infarct volume and BBB damage as compared to the PIS mice treated with Veh (Fig. 6 *B–D*). Meanwhile, the treatment of ISO-1 or Nec-1s markedly reduced TUNEL$^+$ or pRIPK1$^+$ ECs as compared to the Veh treatment in the PIS mice brain (Fig. 6 *E* and *F*). The combination of the inhibition of MIF with ISO-1 and the RIPK1 kinase inhibitor Nec-1s dramatically rescued the BBB disruption and ECs cell death in PIS mice (Fig. 6 *D–F*). Consistently, the neurological assessment by Garcia score also revealed improved total neurological score up to 28 d after PIS in the ISO-1 and Nec-1s treated mice and the combination of these two inhibitors provided further protection (*SI Appendix*, Fig. S7*A*). These data suggest that targeting MIF, RIPK1 kinase activity or combining MIF and RIPK1 inhibition could serve as a promising strategy to preserve cerebromicrovascular EC survival and BBB integrity in CNS pathologies promoted by peripheral inflammation.
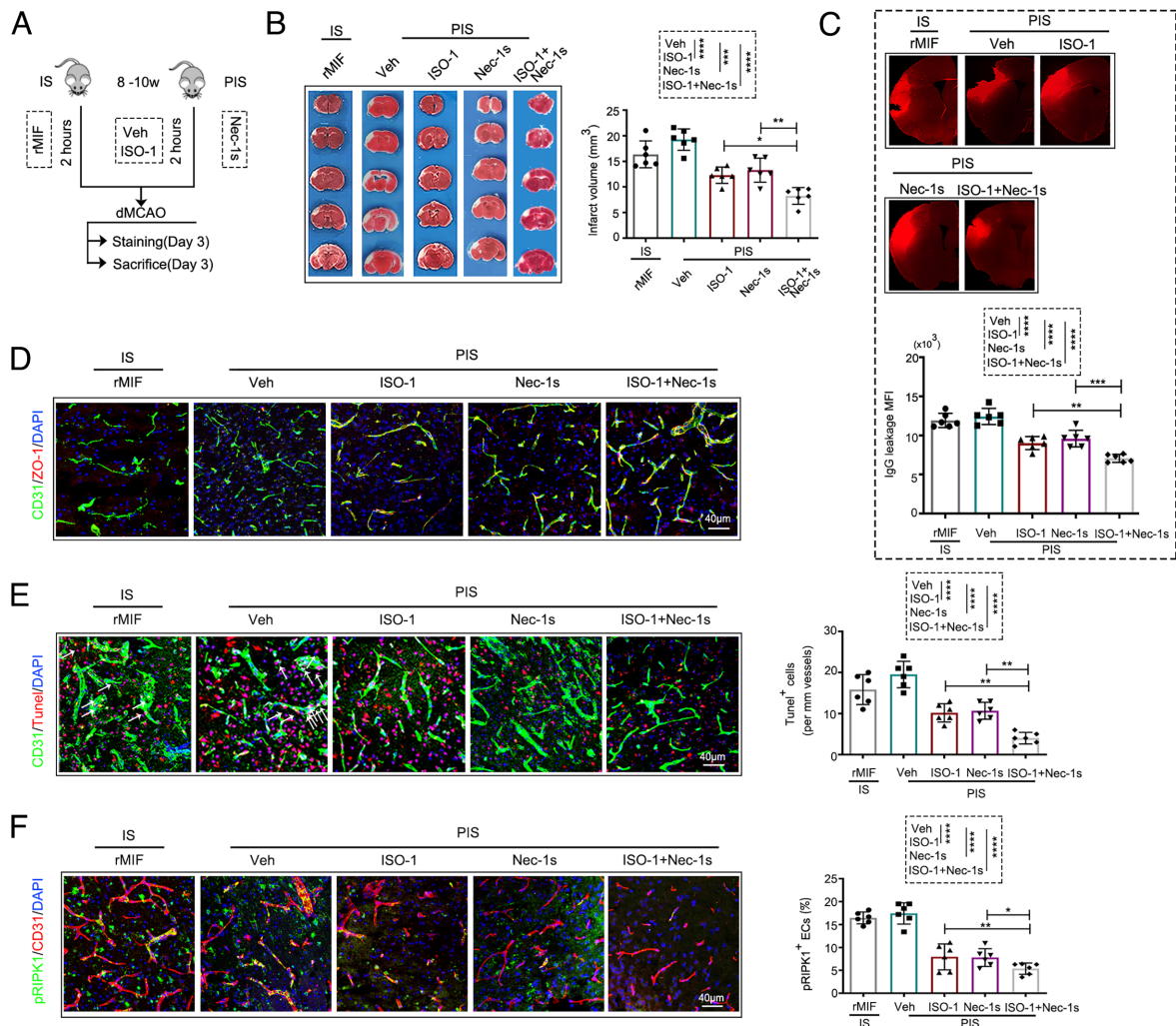
Fig. 6. Inhibition of MIF or RIPK1 reduces PIS-induced BBB damage and neurological deficit. (*A*) Scheme of mice were administered Veh, rMIF, ISO-1, or Nec-1s before dMCAO in PIS mice. (*B*). Representative images (*Left*) and quantification (*Right*) of TTC staining of consecutive coronal sections (1 mm apart) from indicated group 3 d after dMCAO (n = 6 per group, one-way ANOVA with Bonferroni multiple comparisons test). (*C*) Representative images (*Up*) and quantification (*Down*) of IgG extravasation in the ischemic brain from indicated groups 3 d after dMCAO (n = 6 per group, one-way ANOVA with Bonferroni multiple comparisons test). (*D*) Representative confocal images of the tight junction protein ZO-1 and CD31 in brain sections of indicated groups. (Scale bar, 40 μm.) (n = 6 per group, one-way ANOVA with Bonferroni multiple comparisons test). (*E*) Representative confocal images (*Left*) and quantification (*Right*) of TUNEL$^+$CD31$^+$ ECs in brain sections of indicated groups. (Scale bar, 40 μm.) (n = 6 per group, one-way ANOVA with Bonferroni multiple comparisons test). (*F*) Representative confocal images (*Left*) and quantification (*Right*) of pRIPK1(pS166)$^+$CD31$^+$ ECs in brain sections of indicated groups. (Scale bar, 40 μm.) (n = 6 per group, one-way ANOVA with Bonferroni multiple comparisons test). Data are represented as mean ± SD. *$P \leq 0.05$, **$P \leq 0.01$, ***$P \leq 0.001$, ****$P \leq 0.0001$.

Discussion

The present study identified a previously unknown role of myeloid-derived MIF in promoting cerebromicrovascular EC apoptosis and necroptosis by activating RIPK1. Using a clinically relevant PIS model, we demonstrate that surgical trauma-induced sterile inflammation may promote the expression of MIF, which can act as a potent stimulator of cerebromicrovascular EC death and BBB disruption following ischemic brain injury. With genetical and pharmacological evidence, we propose that blocking the release of myeloid MIF or inhibiting the activation of RIPK1 can protect cerebromicrovascular ECs and BBB in the ischemic brain injury.

In this study, we found that MIF could activate RIPK1 in cerebromicrovascular ECs and demonstrated a previously unrecognized mechanism involving inflammation-sensitized EC death. Activation of RIPK1 was previously suggested to induce apoptosis and necroptosis (29). In the present study, we found that the biomarkers of apoptosis (cleaved caspase-3, CC3) and necroptosis (pRIPK3 and pMLKL) were both increased in cerebromicrovascular ECs after PIS. Genetic deletion of myeloid-derived MIF substantially reduced the levels of CC3, pRIPK1, pRIPK3, and pMLKL in ECs, suggesting that myeloid-derived MIF was a potent activator of apoptosis and necroptosis of ECs following PIS. Necroptosis and apoptosis are two distinct regulated cell death mechanisms that have been implicated in mediating neurologic injuries following stroke in ischemic neurons (11). In the current study, using in vivo two-photon imaging, we demonstrated that the adhesion of MIF-loaded myeloid cells were significantly increased following PIS. Notably, we found significantly increased number of pRIPK1$^+$ ECs in PIS mice brain compared to IS mice. Furthermore, the inhibition of RIPK1 kinase by D138N mutation blocked both necroptosis and apoptosis of EC and reduced the BBB disruption after PIS, in which MIF-mediated EC death, suggesting activation of RIPK1 could be one of the mechanisms that underlie MIF-mediated EC death after PIS.

The loss of cerebromicrovascular ECs can damage BBB and impair neurocognitive functions, particularly following sterile inflammation and IS (10, 36). The inflammatory response, which may be triggered by a range of pathogenic stimuli, plays a key role in BBB damage and inducing neurological dysfunction (33). In preclinical models, surgical trauma has been associated with neuroinflammation, cytokine release, and memory dysfunction (32, 37), an important inducer for inflammation (32). As an important initiator of inflammation which has been implicated in various inflammatory-related diseases including IS and surgery, MIF can also mediate cell death under different conditions (24–27). MIF was shown to be increased both in stroke patients and animal models of stroke (38). In the current study, we found that surgical trauma can lead to an increased level of MIF in the plasma, and the increase in peripheral MIF was more pronounced than that with IS alone. However, the role of MIF in the pathogenesis of cerebromicrovascular EC death and the underlying regulatory mechanism has not been explored. In the present study, using an in vivo mice model of PIS, in which a prior surgical trauma exacerbates the extent of a subsequent cerebral ischemic brain injury event, we reveal that peripheral myeloid-derived MIF is pathogenically involved in cerebromicrovascular EC death via activating RIPK1 and promotes BBB disruption and exacerbated neurological deficits after PIS. Compared to other mechanisms of BBB disruption, such as tight junction loss or dysfunctional transcytosis, EC death may represent a mechanism under severe brain injury.

Over the past decades, compelling evidence suggests that the consequence of a surgery includes chronic, low-grade inflammation but the mechanism remains under-investigated (32, 39).

The present study reveals a rapid and significant elevation of MIF in the circulation and peripheral myeloid cells in clinical surgical patients. Strikingly, the MIF production in myeloid cells (mainly macrophages) was increased in mice after surgery trauma and PIS, but not in neutrophil or spleen, suggesting macrophages are the most sensitive responder to surgery. Notably, when we compared the potential impact of the other perioperative factors, such as stress, pain and trauma on the MIF expression by flow cytometry, we found that the elevation in the production of macrophagic MIF was most sensitive to surgical trauma rather than stress or pain. Microglia, as innate immune cells homologous to macrophages in the CNS, may also be activated after PIS. However, the activation of microglia in the brain is indirectly caused by surgical trauma, and may synergistically promote inflammatory response caused by surgical trauma and neuroinflammation in the brain. The MIF released by macrophages in peripheral blood can be directly induced by surgical trauma alone.

Peripheral myeloid cells can be recruited to the area of ischemic brain injury by CCR2 and other chemokine receptors (40, 41). Local MIF levels in cerebral ECs may be significantly increased when MIF loaded myeloid cells adhere and aggregate on the cerebromicrovascular ECs after PIS, thus generating a vicious circle aggravating post-PIS brain damage (42). However, it is difficult to address locally increased MIF level around cerebromicrovascular ECs after PIS. Taking advantage of MIF$^{\Delta Lyz2}$ mice, we show that myeloid-specific loss of MIF significantly reduces EC death, BBB leakage, and neurological dysfunction after PIS, supporting the key role of myeloid-derived MIF in cerebromicrovascular EC death. Of note, both our in vivo and in vitro experiments suggest that surgery alone or MIF alone does not initiate EC death. The role of MIF is to exacerbate and sensitize cerebromicrovascular ECs to RDA and necroptosis in the context of ischemic injury. However, we currently cannot exclude the effect of peripheral myeloid-derived MIF on other cell types in ischemic brain after PIS, which deserves further exploration.

The inhibition of MIF or RIPK1 by ISO-1 and Nec-1s, respectively, could reduce EC death, BBB disruption after PIS, potentially providing therapeutic benefits for PIS. Previous studies found the efficacies of ISO-1 or Nec-1s in the animal models of immune-inflammatory diseases and CNS diseases improvements such as rheumatoid arthritis, SARS-CoV-2, atherosclerosis, amyotrophic lateral sclerosis, Alzheimer's disease and Parkinson (15, 28, 43, 44), suggesting that MIF and RIPK1 are attractive therapeutic targets for the treatment of inflammatory and neurodegenerative diseases. Furthermore, our study suggests that a combination strategy of targeting both MIF and RIPK1 may be potentially more effective therapeutically than single agent alone. The underlying mechanisms and the application in clinical paradigms require further investigation.

Collectively, the current study reveals a previously unrecognized EC death mechanism in which MIF promotes ECs apoptosis and necroptosis through RIPK1-dependent pathway. The above finding may increase the understanding how peripheral inflammation promotes CNS pathology. MIF and RIPK1 can serve as promising therapeutic targets for preserving cerebromicrovascular EC survival and BBB integrity in CNS pathologies promoted by peripheral inflammation, such as PIS.

Materials and Methods

The clinical study was approved by the ethical review board of Renji Hospital of Shanghai Jiaotong University (KY2019-168) and was performed according to

the Declaration of Helsinki. Informed consent was obtained from all patients or legally authorized representatives. Baseline characteristics of patients recruited in the prospective cohort were listed in the *SI Appendix*, Table S1. Key resources that are essential to reproduce the above experimental results are listed in *SI Appendix*, Table S2. PIS mice model was induced in adult male C57/BL6 mice (8 to 10 wk old, 25 to 30 g). All animal procedures were approved by the Institutional Animal Care and Use Committee of Renji Hospital, Shanghai Jiaotong University School of Medicine in accordance with the Guide for the Care and Use of Laboratory Animals. For detailed methodological information, please refer to the *SI Appendix*.

Data, Materials, and Software Availability. All datasets are included in the article and/or *SI Appendix*.

Author affiliations: [a]Department of Anesthesiology, Clinical Research Center, Renji Hospital, Shanghai Jiao Tong University School of Medicine, Shanghai 200127, China; [b]Interdisciplinary Research Center on Biology and Chemistry, Shanghai Institute of Organic Chemistry, Shanghai 201210, China; [c]Shanghai Key Laboratory of Aging Studies, Shanghai, 201210 China; [d]Department of Neurosurgery, Renji Hospital, Shanghai Jiao Tong University School of Medicine, Shanghai 200127, China; and [e]Department of Radiology, Renji Hospital, Shanghai Jiao Tong University School of Medicine, Shanghai 200127, China

1. G. A. Mashour, L. E. Moore, A. V. Lele, S. A. Robicsek, A. W. Gelb, Perioperative care of patients at high risk for stroke during or after non-cardiac, non-neurologic surgery: Consensus statement from the Society for Neuroscience in Anesthesiology and Critical Care*. *J. Neurosurg. Anesthesiol.* **26**, 273–285 (2014).
2. S. O. Algra *et al.*, Cerebral ischemia initiates an immediate innate immune response in neonates during cardiac surgery. *J. Neuroinflammation* **10**, 24 (2013).
3. P. Vlisides, G. Mashour, Perioperative stroke. *Canadian J. Anaesth. J. Canadien d'anesthesie* **63**, 193–204 (2016).
4. P. Vlisides, G. A. Mashour, Perioperative stroke. *Can. J. Anaesth.* **63**, 193–204 (2016).
5. M. Fischer, U. Kahl, Perioperative stroke. *Anaesthesist* **70**, 3–12 (2021).
6. M. D. Sweeney, A. P. Sagare, B. V. Zlokovic, Blood-brain barrier breakdown in Alzheimer disease and other neurodegenerative disorders. *Nat. Rev. Neurol.* **14**, 133–150 (2018).
7. M. D. Sweeney, Z. Zhao, A. Montagne, A. R. Nelson, B. V. Zlokovic, Blood-Brain barrier: From Physiology to disease and back. *Physiol. Rev.* **99**, 21–78 (2019).
8. A. Montagne *et al.*, APOE4 leads to blood-brain barrier dysfunction predicting cognitive decline. *Nature* **581**, 71–76 (2020).
9. D. A. Nation *et al.*, Blood-brain barrier breakdown is an early biomarker of human cognitive dysfunction. *Nat. Med.* **25**, 270–276 (2019).
10. L. J. Trigiani *et al.*, A functional cerebral endothelium is necessary to protect against cognitive decline. *J. Cereb. Blood Flow Metab.* **42**, 74–89 (2021), 10.1177/0271678X211045438, 271678X211045438
11. R. N. Munji *et al.*, Profiling the mouse brain endothelial transcriptome in health and disease models reveals a core blood-brain barrier dysfunction module. *Nat. Neurosci.* **22**, 1892–1902 (2019).
12. J. Hauptmann *et al.*, Interleukin-1 promotes autoimmune neuroinflammation by suppressing endothelial heme oxygenase-1 at the blood-brain barrier. *Acta Neuropathol.* **140**, 549–567 (2020).
13. Y. Wu *et al.*, von Willebrand factor enhances microvesicle-induced vascular leakage and coagulopathy in mice with traumatic brain injury. *Blood* **132**, 1075–1084 (2018).
14. J. M. Lord *et al.*, The systemic immune response to trauma: An overview of pathophysiology and treatment. *Lancet* **384**, 1455–1465 (2014).
15. E. F. Morand, M. Leech, J. Bernhagen, MIF: A new cytokine link between rheumatoid arthritis and atherosclerosis. *Nat. Rev. Drug Discov.* **5**, 399–410 (2006).
16. K. Sumaiya, D. Langford, K. Natarajaseenivasan, S. Shanmughapriya, Macrophage migration inhibitory factor (MIF): A multifaceted cytokine regulated by genetic and physiological strategies. *Pharmacol. Ther.* **233**, 108024 (2022).
17. A. Zernecke, J. Bernhagen, C. Weber, Macrophage migration inhibitory factor in cardiovascular disease. *Circulation* **117**, 1594–1602 (2008).
18. H. Park *et al.*, PAAN/MIF nuclease inhibition prevents neurodegeneration in Parkinson's disease. *Cell* **185**, 1943–1959 e1921 (2022).
19. T. Nyunt *et al.*, Mitochondrial oxidative stress-induced transcript variants of ATF3 mediate lipotoxic brain microvascular injury. *Free Radic. Biol. Med.* **143**, 25–46 (2019).
20. O. de Montgolfier *et al.*, High systolic blood pressure induces cerebral microvascular endothelial dysfunction, neurovascular unit damage, and cognitive decline in mice. *Hypertension* **73**, 217–228 (2019).
21. H. Wang *et al.*, NEK1-mediated retromer trafficking promotes blood-brain barrier integrity by regulating glucose metabolism and RIPK1 activation. *Nat. Commun.* **12**, 4826 (2021).
22. Y. Li *et al.*, Aging neurovascular unit and potential role of DNA damage and repair in combating vascular and neurodegenerative disorders. *Front. Neurosci.* **13**, 778 (2019).
23. A. Baeza Garcia *et al.*, Neutralization of the plasmodium-encoded MIF ortholog confers protective immunity against malaria infection. *Nat. Commun.* **9**, 2714 (2018).
24. C. Stoppe *et al.*, The protective role of macrophage migration inhibitory factor in acute kidney injury after cardiac surgery. *Sci. Transl. Med.* **10**, 4886 (2018).
25. K. Sumaiya, D. Langford, K. Natarajaseenivasan, S. Shanmughapriya, Macrophage migration inhibitory factor (MIF): A multifaceted cytokine regulated by genetic and physiological strategies. *Pharmacol. Ther.* **233**, 108024 (2021), 10.1016/j.pharmthera.2021.108024.
26. Y. Wang, A nuclease that mediates cell death induced by DNA damage and poly(ADP-ribose) polymerase-1. *Sci. (New York, N.Y.)* **354**, aad6872 (2016).
27. A. A. Vandenbark, R. Meza-Romero, G. Benedek, H. Offner, A novel neurotherapeutic for multiple sclerosis, ischemic injury, methamphetamine addiction, and traumatic brain injury. *J. Neuroinflammation* **16**, 14 (2019).
28. J. Yuan, P. Amin, D. Ofengeim, Necroptosis and RIPK1-mediated neuroinflammation in CNS diseases. *Nat. Rev. Neurosci.* **20**, 19–33 (2019).
29. L. Mifflin, D. Ofengeim, J. Yuan, Receptor-interacting protein kinase 1 (RIPK1) as a therapeutic target. *Nat. Rev. Drug Discovery* **19**, 553–571 (2020).
30. M. G. Naito *et al.*, Sequential activation of necroptosis and apoptosis cooperates to mediate vascular and neural pathology in stroke. *Proc. Natl. Acad. Sci. U.S.A.* **117**, 4959–4970 (2020).
31. A. Degterev *et al.*, Chemical inhibitor of nonapoptotic cell death with therapeutic potential for ischemic brain injury. *Nat. Chem. Biol.* **1**, 112–119 (2005).
32. T. Yang, R. Velagapudi, N. Terrando, Neuroinflammation after surgery: From mechanisms to therapeutic targets. *Nat. Immunol.* **21**, 1319–1326 (2020).
33. J. V. Pluvinage, T. Wyss-Coray, Systemic factors as mediators of brain homeostasis, ageing and neurodegeneration. *Nat. Rev. Neurosci.* **21**, 93–102 (2020).
34. J. B. Ruden *et al.*, Reduction of leukocyte microvascular adherence and preservation of blood-brain barrier function by superoxide-lowering therapies in a piglet model of neonatal asphyxia. *Front. Neurol.* **10**, 447 (2019).
35. T. P. Santisakultarm *et al.*, Stalled cerebral capillary blood flow in mouse models of essential thrombocythemia and polycythemia vera revealed by in vivo two-photon imaging. *J. Thromb. Haemost.* **12**, 2120–2130 (2014).
36. Y. Shi *et al.*, Endothelium-targeted overexpression of heat shock protein 27 ameliorates blood-brain barrier disruption after ischemic brain injury. *Proc. Natl. Acad. Sci. U.S.A.* **114**, E1243–E1252 (2017).
37. G. Luo *et al.*, Metabolic reprogramming mediates hippocampal microglial M1 polarization in response to surgical trauma causing perioperative neurocognitive disorders. *J. Neuroinflammation* **18**, 267 (2021).
38. Y. C. Liu *et al.*, Cytokine MIF enhances blood-brain barrier permeability: Impact for therapy in ischemic stroke. *Sci. Rep.* **8**, 743 (2018).
39. J. Rossaint, A. Margraf, A. Zarbock, Perioperative inflammation. *Anaesthesist* **68**, 421–427 (2019).
40. G. U. Enzmann, S. Pavlidou, M. Vaas, J. Klohs, B. Engelhardt, ICAM-1(null) C57BL/6 mice are not protected from experimental ischemic stroke. *Transl. Stroke Res.* **9**, 608–621 (2018).
41. P. Sun *et al.*, Inhibition of calcium/calmodulin-dependent protein kinase kinase (CaMKK) exacerbates impairment of endothelial cell and blood-brain barrier after stroke. *Eur. J. Neurosci.* **49**, 27–39 (2019).
42. M. A. Moskowitz, E. H. Lo, C. Iadecola, The science of stroke: Mechanisms in search of treatments. *Neuron* **67**, 181–198 (2010).
43. G. Xu *et al.*, SARS-CoV-2 promotes RIPK1 activation to facilitate viral propagation. *Cell Res.* **31**, 1230–1243 (2021).
44. L. Mifflin *et al.*, A RIPK1-regulated inflammatory microglial state in amyotrophic lateral sclerosis. *Proc. Natl. Acad. Sci. U.S.A.* **118**, e2025102118 (2021).